Bioorg. Med. Chem. 99 (2024) 117597

Contents lists available at ScienceDirect

Bioorganic & Medicinal Chemistry

journal homepage: www.elsevier.com/locate/bmc

Selective targeting of human TET1 by cyclic peptide inhibitors: Insights from biochemical profiling

Klemensas Šimelis [a], Hilal Saraç [b], Eidarus Salah [a], Kosuke Nishio [c], Tom E. McAllister [b], Thomas P. Corner [a], Anthony Tumber [a], Roman Belle [a,b], Christopher J. Schofield [a], Hiroaki Suga [c], Akane Kawamura [a,b,*]

[a] Chemistry Research Laboratory, Department of Chemistry and the Ineos Oxford Institute for Antimicrobial Research, University of Oxford, 12 Mansfield Road, OX1 3TA Oxford, United Kingdom
[b] Chemistry - School of Natural and Environmental Sciences, Newcastle University, Bedson Building, NE1 7RU Newcastle upon Tyne, United Kingdom
[c] Department of Chemistry, Graduate School of Science, The University of Tokyo, 7-3-1 Hongo, Bunkyo-ku, Tokyo 113-0033, Japan

A B S T R A C T

Ten-Eleven Translocation (TET) enzymes are Fe(II)/2OG-dependent oxygenases that play important roles in epigenetic regulation, but selective inhibition of the TETs is an unmet challenge. We describe the profiling of previously identified TET1-binding macrocyclic peptides. TiP1 is established as a potent TET1 inhibitor (IC_{50} = 0.26 μM) with excellent selectivity over other TETs and 2OG oxygenases. TiP1 alanine scanning reveals the critical roles of Trp10 and Glu11 residues for inhibition of TET isoenzymes. The results highlight the utility of the RaPID method to identify potent enzyme inhibitors with selectivity over closely related paralogues. The structure–activity relationship data generated herein may find utility in the development of chemical probes for the TETs.

1. Introduction

Epigenetic modification of chromatin plays an important role in the regulation of eukaryotic gene expression and subsequent phenotype presentation.[1] The Ten-Eleven Translocation (TET) enzymes, which belong to the Fe(II)- and 2-oxoglutarate (2OG)-dependent oxygenase superfamily, are responsible for the deposition of cytosine-based modifications to DNA. The TETs utilise 2OG and O_2 as co-substrates to sequentially oxidise 5-methylcytosine (^{5m}C) to 5-hydroxymethylcytosine (^{5hm}C), 5–formylcytosine (^{5f}C), and 5-carboxycytosine (^{5ca}C), releasing succinate and CO_2 as by-products (Fig. 1A).[2,3] The oxidised forms of ^{5m}C are epigenetic marks with distinct enrichment patterns and are proposed intermediates in cytosine demethylation.[4–10] In humans, there are three TET paralogues, which share high sequence identity within the catalytic domain (Fig. 1B). However, their highly differentiated *N*– and *C*–terminal regions and apparently specific DNA sequence preferences suggest divergent biological roles.[11–13] In addition to their enzymatic functions, the TETs have been reported to serve as transcriptional co-activators/co-repressors by interacting with transcriptional regulators and scaffolding proteins,[14] such as histone deacetylases[15] or the SIN3A co-repressor complex.[16] The ^{5m}C hydroxylase and protein recruitment functions of TETs are crucial in developmental processes, such as pre-implantation development,[17] genomic imprinting erasure,[18] and pluripotency regulation.[19,20] TET dysfunction is implicated in a number of oncological conditions: decreased TET protein and ^{5hm}C levels are associated with breast, liver, lung, pancreatic, and prostate cancers,[21] while *TET2* loss-of-function mutations are prevalent in haematopoietic malignancies,[22] most notably acute myeloid leukaemia.[23]

Despite the pivotal roles of TETs in mammalian development and cancer progression, there remains a dearth of paralogue-specific TET inhibitors for the exploration of their distinct biological functions. The majority of TET inhibitors available to-date inhibit 2OG oxygenases with pan-specific activity, such as the 2OG mimetic *N*–oxalylglycine (NOG)[28,29] and 2OG competitive metal chelators IOX1 (ref.[30]) and 2,4-PDCA.[31,32] While TETi76, a 2-hydroxyglutarate derivative, showed excellent selectivity for TETs over other 2OG oxygenase families, it has only 6-fold selectivity within the TET family.[33] We previously reported the use of mRNA display-based random nonstandard peptide integrated discovery (RaPID) display to identify macrocyclic peptide inhibitors of TET1.[34] One of peptides, TiP1, exhibited promising selectivity for TET1 over TET2. However, TiP1 was not evaluated for inhibition of TET3 or other members of the superfamily, and a number of other sequences identified using the RaPID system remained uncharacterised.[33] Here, we

* Corresponding author at: Chemistry - School of Natural and Environmental Sciences, Newcastle University, Bedson Building, NE1 7RU Newcastle upon Tyne, United Kingdom.
E-mail address: akane.kawamura@newcastle.ac.uk (A. Kawamura).

https://doi.org/10.1016/j.bmc.2024.117597
Received 27 November 2023; Received in revised form 8 January 2024; Accepted 10 January 2024
Available online 12 January 2024

provide a more comprehensive selectivity profiling of TiP1 and other peptides against a panel of 2OG oxygenases. Our findings reveal excellent selectivity of TiP1 for TET1 over other TET paralogues (>20-fold) and representative 2OG oxygenases (>40-fold). We identify key residues essential for TiP1 potency against TETs and validate *C*–terminal elongation as a strategy for installing functional handles. Additionally, TiP1 and its conjugates with cell-penetrating peptides are tested for cellular activity.

2. Results

2.1. Characterisation of cyclic peptide hits against a panel of 2OG oxygenases

Previously, we reported the use of RaPID display to screen a library of thioether cyclised peptides (Scheme S1) against the compact catalytic domain of TET1 and identified hit sequences using traditional cloning and Sanger sequencing methods.[34] This gave rise to eight peptides (TiP1–8), three of which were confirmed to be binders and catalytic inhibitors of TET1 (TiP1–3). In this study, the enriched sequences from the TET1 RaPID selection[34] using D-Tyr and D-Trp NNK libraries were further analysed using next-generation sequencing (NGS) to explore additional TET-binding sequences. The top 20 most abundant peptide sequences in the final round of each selection are shown in Tables S1 and S2, representing 85% and 88% of the sequence pools in the D-Tyr and D-Trp selections, respectively. Thirteen cyclic peptides were selected on the basis of enrichment in the final round of selection and peptide sequence diversity and, together with the previous TiP1–3 hits, were synthesised using solid-phase peptide synthesis (Table S3). These peptides were then tested as inhibitors of human TET1–3 and murine Tet1 (mTet1), a closely related homologue of human TET1 (catalytic domain similarity 65.6%), using luminescence-based AlphaScreen (AS) biochemical assay (Figs. S1, S2A, B).[32] TiP1 demonstrated excellent selectivity for TET1 within the TET recombinant catalytic domain (CD) panel, displaying >20-fold higher potency for TET1 (IC_{50} = 260 nM) compared to TET2, TET3, and mTet1 (Fig. 2A, B, E, Table S4). By contrast, the linearised form of TiP1 (TiP1.L) exhibited 250-fold lower potency for TET1 and poor selectivity, underscoring that conformational rigidity induced by cyclisation is crucial for inhibitory activity. The majority of the tested peptides showed inhibition of TET1 by the AS assay, with IC_{50} values between 200 nM and 2 μM (Table S4). However, AS signal suppression was also observed in an enzyme-free AS interference assay designed to identify false-positive hits. While minimal AS signal interference was observed for IOX1, TiP1, TIP1.L, KS03, KS08, and KS09 (Fig. S3), other peptides suppressed the assay signal to varying degrees (EC_{50} range 0.83–31 μM, Table S4), precluding the accurate evaluation of their potency and selectivity profiles using AS assay. To mitigate this issue, the peptides were tested using an orthogonal solid-phase extraction-mass spectrometry (SPE-MS) assay which directly measures the rate of TET-catalysed oxidation of ^{5m}C to ^{5hm}C in DNA oligomers (Fig. S2C, D). SPE-MS assay was only suitable for evaluating the inhibition of TET2, but not TET1 or TET3, due to the considerably higher enzyme requirement compared to AS assay. Some variability was observed between the IC_{50} values obtained using the two orthogonal assays for TET2 (Fig. 2C, E, Table S5), likely due to differences in the assay conditions, but TET1 selectivity over TET2 was retained for TiP1 (>20-fold) and KS08 (12-fold).

The cyclic peptide TiP1 was selected for further characterisation due to its high potency against TET1, excellent selectivity within the TET family, and expedient synthesis relative to other peptides. Cross-screening of TiP1 against representative 2OG oxygenases revealed >90-fold selectivity for TET1 over histone lysine demethylases KDM5B and KDM6B and hypoxia-inducible factor prolyl hydroxylase 2 (PHD2),[35] as well as >40-fold selectivity over asparaginyl hydroxylase FIH[35] and asparaginyl/aspartyl hydroxylase ASPH,[36] establishing TiP1 as a TET1-selective inhibitor (Fig. 2D, E).

2.2. TiP1 structure–activity relationship investigation using alanine scanning

In order to investigate the influence of specific residues on the inhibitory properties of TiP1, an alanine scan was carried out. Alanine variants for every non-Ala residue except the terminal residues were synthesised (Table S3) and screened for signal interference and TET1–3 inhibition using AS assay. The majority of alanine variants showed at least a 3-fold reduction in TET1 inhibitory potency compared to TiP1 (Fig. 3, Table S6), confirming that the peptide sequences identified using the RaPID system were highly optimised for TET1 binding. By contrast,

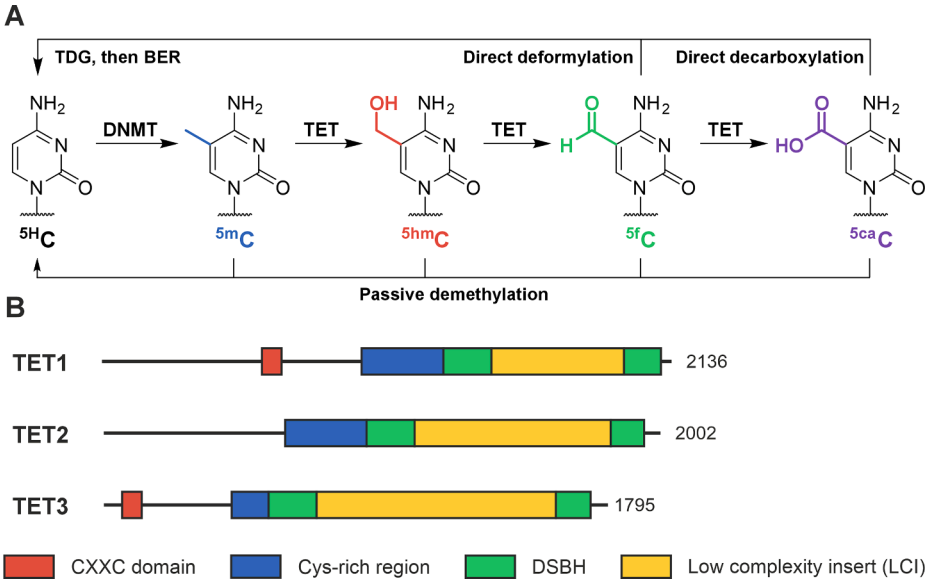

Fig. 1. TETs and their involvement in ^{5m}C demethylation pathways. A, Dynamic cytosine modification pathways. Cytosine is methylated by DNA methyltransferases (DNMTs) to produce ^{5m}C, which can be iteratively oxidised to ^{5hm}C, ^{5f}C, and ^{5ca}C by TETs in an Fe(II)/2OG-dependent manner.[3] ^{5f}C and ^{5ca}C can be replaced with unmodified ^{5H}C via passive demethylation, TDG/BER mechanisms,[24] direct deformylation,[25] or decarboxylation.[26,27] **B**, Domain architecture of full-length human TETs. DSBH, double-stranded β-helix.

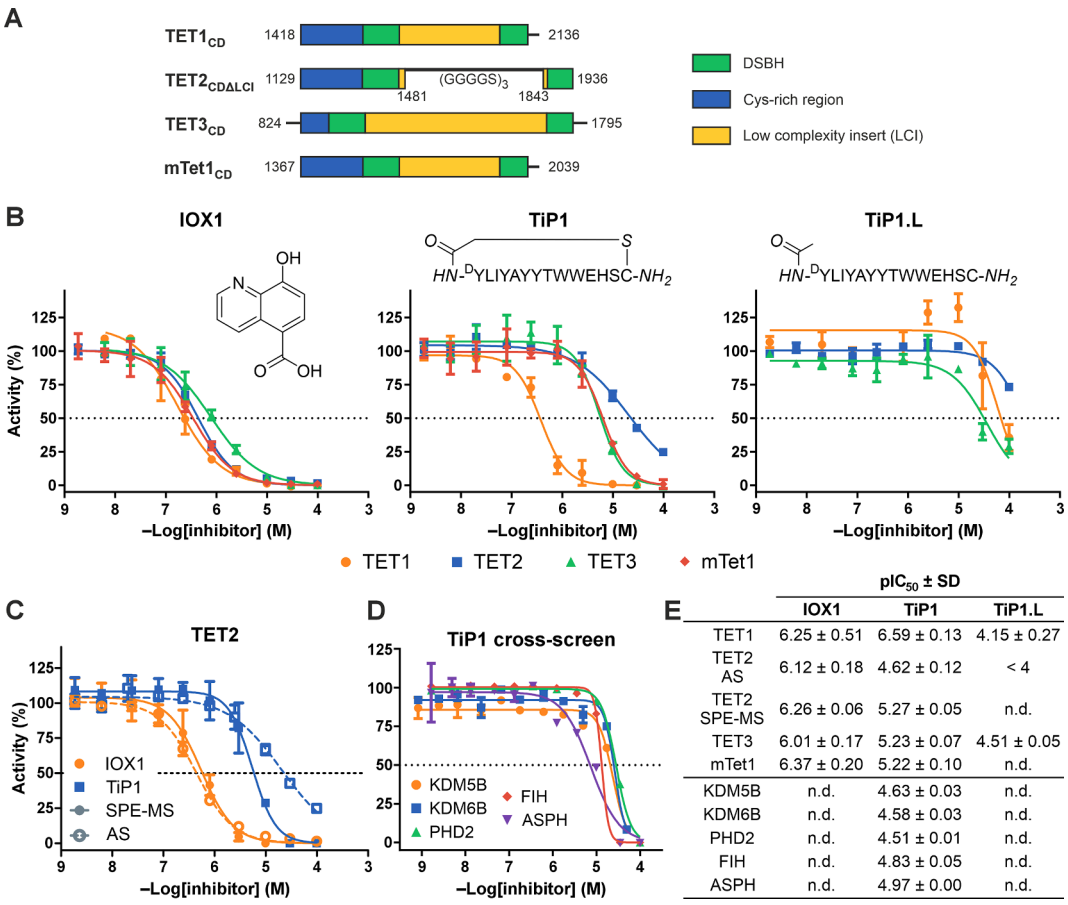

Fig. 2. Inhibitory activity profiling of TiP1. A, Domain architecture of TET constructs used in this study. **B**, Representative AlphaScreen (AS) assay dose–response curves of TET1–3 and mTet1 inhibition by broad-spectrum 2OG oxygenase inhibitor IOX1, cyclic peptide TiP1, and its linear analogue TiP1.L. **C**, Representative AS and SPE-MS assay dose–response curves of TET2 inhibition by IOX1 and TiP1. **D**, Representative dose–response curves for TiP1 cross-screening against a panel of 2OG oxygenases. **E**, pIC_{50} values. Dose-response curves are shown as the means of n experimental replicates (TET AS, n = 2–3; TET SPE-MS, KDM5B/6B, PHD2, FIH, ASPH, n = 2; mean ± SD). Tabulated data are the means of n independent replicates (AS IOX1, n = 6–9; AS TiP1, n = 2–6; AS TiP1.L, n = 3; SPE-MS, n = 2; mean ± SD). Italicised letters in schematic representations of TiP1 and TiP1.L represent individual atoms. DSBH, double-stranded β-helix. n.d., not determined. AS, AlphaScreen. SPE-MS, solid-phase extraction-mass spectrometry.

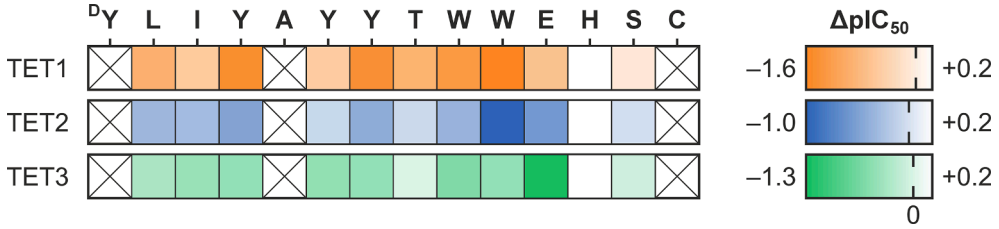

Fig. 3. Characterisation of TiP1 alanine variants using AlphaScreen assays. TET1–3 inhibitory potencies of the variants are visualised as pIC_{50} value shifts relative to parent peptide TiP1. Data are reported as the means of three independent replicates (n = 3; mean ± SD).

changes in potency for TET2/TET3 were less pronounced, consistent with the selectivity profile of TiP1 (Fig. 2B). Substitutions at Tyr4, Tyr7, and Trp10 had the highest impact (>25-fold potency loss), with Trp10 emerging as a key residue for the inhibition of TET1 and TET2 (42-fold and approx. 10-fold potency loss for W10A, respectively). Notably, Glu11, but not Trp10, was essential for TET3 inhibition (>20-fold potency loss for E11A), highlighting distinctions in the peptide binding site features within the TET family. H12A and S13A substitutions produced only marginal potency changes (<2-fold) across the TET panel, suggesting that residues proximal to the thioether linkage are not directly involved in protein binding.

2.3. Evaluation of TiP1 and TiP1 conjugate cellular activity

To explore the potential utility of TiP1 as a chemical tool, we tested it in cellular assays.[32] These utilised U2OS cells stably transfected with a dox-inducible FLAG-tagged catalytic domain of TET1, enabling transient expression of TET1 and enrichment of ^{5m}C oxidation products, in particular ^{5hm}C (Fig. S4A). IOX1 inhibited TET1 activity in cells (IC_{50} = 22 μM, Fig. S4B), in line with a previous report.[37] By contrast, TiP1 did not produce a dose-dependent reduction in ^{5hm}C levels in cells overexpressing TET1 (Fig. S4B), but increased FLAG staining and reduced cell number, indicating cytotoxicity. The lack of dose-dependent catalytic inhibition may be attributed to poor membrane permeability, a common challenge associated with macrocyclic peptides.[38,39] Given the

results of the TiP1 alanine scan, sequence-based optimisation of TiP1 physiochemical properties to improve permeability may be challenging.

The conjugation of TiP1 with cell-penetrating peptides (CPPs) was then explored as an alternative strategy. TiP1 was modified by conjugation of two reported cationic CPP sequences (R8 or TAT),[40] as well as an anionic FLAG sequence as a control (Fig. 4A). Addition of the FLAG sequence did not affect the potency against recombinant TET1 using AS assay (TiP1-FLAG, Figs. 4B–D and S5, Table S7) and improved selectivity for TET1 over TET3 (58-fold and 23-fold for TiP1-FLAG and TiP1, respectively). TiP1-TAT was a substantially more potent TET1 inhibitor compared to TiP1 (IC_{50} = 18 and 260 nM for TiP1-TAT and TiP1, respectively), but exhibited reduced selectivity within the TET family (≤10-fold selective, Figs. 4D and S5). Interestingly, FLAG peptide alone did not affect recombinant TET activity, whereas the basic TAT and R8 peptides alone were found to inhibit TET1 and TET2 (IC_{50} = 0.25–4 μM; Fig. 4C, D), but not TET3 (IC_{50} >100 μM). Although the cationic nature of the CPPs raises concerns over non-specific binding to the substrate DNA backbone, TAT and R8 peptides produced minimal AS signal interference under the conditions tested (Fig. S5). However, it is possible that CPPs may negatively affect substrate binding to the TETs.

TiP1 and the three TiP1 derivatives were tested for activity in cells, using IOX1 as a positive control (Fig. S4C–E). While TiP1-FLAG was less cytotoxic than the parent peptide, conjugation with TAT or R8 CPPs promoted cytotoxicity, in agreement with a previous report involving an R9 conjugate of KDM4A inhibitor CP2.[41] For TiP1-TAT and TiP1-R8, some reduction in ^{5hm}C levels was observed at the highest concentrations tested (50–100 μM), although off-target effects resulting from cytotoxicity cannot be ruled out. Negligible changes were observed for TiP1 or TiP1-FLAG to ^{5hm}C levels.

3. Discussion

In summary, we synthesised a set of 16 macrocyclic peptides from a TET1 RaPID display[34] and profiled their inhibitory potencies against TET enzymes using biochemical assays. Following further characterisation, TiP1 was established as the first inhibitor to be selective for a single TET paralogue with >20-fold selectivity over other TETs (TET2/3) and up to >100-fold selectivity over five representative 2OG oxygenases. Evaluation of single alanine variants of TiP1 implied poor tolerance to peptide sequence modification with respect to TET1 inhibition, but not for inhibition of TET2 or TET3. The aromatic side chains Tyr4, Tyr7, and Trp10 of TiP1 are crucial for TET1 inhibition.[42] Interestingly, Glu11 of TiP1 emerged as being important for TET3 inhibition, indicating the possibility of a hydrogen bonding interaction between TiP1 and TET3 not present in other TET paralogues. While further work is needed to ascertain the exact binding site and the mode of inhibition, TiP1 provides a unique chemical tool for selectively studying TET1. TiP1 is complementary to the less selective reported small molecule inhibitors that are competitive with respect to 2OG and chelate the catalytic Fe(II).[28–34]

TiP1 did not elicit an inhibitory response in U2OS cells overexpressing TET1 and was cytotoxic at concentrations above 100 μM

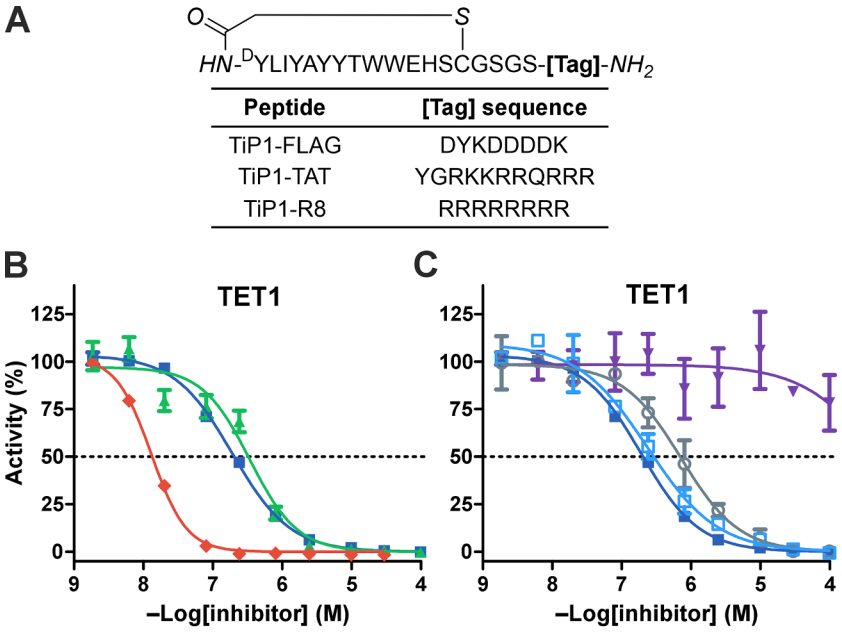

Peptide	[Tag] sequence
TiP1-FLAG	DYKDDDDK
TiP1-TAT	YGRKKRRQRRR
TiP1-R8	RRRRRRRR

D

		pIC_{50} ± SD		
		TET1	TET2	TET3
■	TiP1	6.59 ± 0.13	4.62 ± 0.12	5.23 ± 0.07
▲	TiP1-FLAG	6.39 ± 0.06	4.59 ± 0.08	4.63 ± 0.05
◆	TiP1-TAT	7.74 ± 0.21	6.91 ± 0.00	6.74 ± 0.05
–	TiP1-R8	n.d.	n.d.	n.d.
▼	FLAG	< 4	< 4	< 4
○	TAT	5.94 ± 0.20	5.39 ± 0.25	< 4
□	R8	6.60 ± 0.02	6.45 ± 0.59	< 4

Fig. 4. Inhibitory activity profiling of TiP1 conjugates. A, Schematic representation of TiP1 conjugate structures (italicised letters represent individual atoms). Representative AS dose–response curves of TET1 inhibition by (**B**) TiP1 conjugates and (**C**) tag-only controls. **D**, pIC_{50} values. Dose-response curves are shown as the means of two experimental replicates (n = 2; mean ± SD). Tabulated data are the means of three independent replicates (n = 3, mean ± SD). n.d., not determined.

(Fig. S4). Derivatisation of the *C*–terminus of TiP1 with cell-penetrating cationic peptides (TAT or R8) led to a reduction in cellular ^{5hm}C levels at higher concentrations (30–100 μM), although further work is necessary to elucidate the mechanism of action underlying this observation, including with respect to toxicity.

Although the cellular activity of TiP1 and its CPP conjugates is unclear, the biochemical SAR data generated herein may serve as a valuable reference point for the future design of cell-active TET cyclic peptide inhibitors, small molecule peptidomimetics, or small molecule leads, as successfully exemplified in peptide-derived cell-active inhibitors for severe acute respiratory syndrome-coronavirus (SARS-CoV) proteases and von Hippel-Lindau (VHL) ligands.[43,44] TiP1-based affinity probes, such as TiP1-FLAG, may also find utility in TET interactome mapping (e.g. proteomics).[45,46] Selective TET1 inhibitors could potentially be further developed towards cancer therapeutics, as upregulation of TET1 has been implicated as a driver of hepatoblastoma,[47] hepatocellular carcinoma,[48] and breast cancer.[49,50] Overall, the results highlight the utility of the RaPID method to identify potent enzyme inhibitors with selectivity over closely related paralogues. The excellent selectivity profile of TiP1 supports its potential utility as a chemical tool to probe the biology of TET1.

4. Materials and methods

4.1. Materials

OxymaPure (Merck, Cat# 8510860250), *N*,*N*'–diisopropylcarbodiimide (DIC, Merck, Cat# 803649), DMF and 20% piperidine in DMF (for peptide synthesis, Merck, Cat# 1,003,972,500 and Cat# 80645-2L, respectively), sodium trimethylsilane propionate (TSP-[^{2}H]$_4$, Sigma, Cat# 269913-1G), (+)-sodium L-ascorbate (Sigma, Cat#: 11140), $(NH_4)_2Fe(SO_4)_2$ (Sigma, Cat#: 215406-100G), disodium 2-oxoglutarate (2OG, Sigma, Cat#: K3752-100G), ProxiPlate™, White Shallow-well, 384-well (PerkinElmer, Cat# 6008350), DTPA purified 7.5% Bovine Serum Albumin solution (SA, PerkinElmer, Cat# CR84-10), AlphaScreen General IgG (Protein A) Detection Kit (PerkinElmer, Cat# 6760617), Greiner Microplate, 384 well (PP, V-bottom, Cat# 781280), Tween® 20 (Promega, Cat# H5151), ^{5m}C or ^{5hm}C single-stranded DNA (5′-[Biotin]- TCG GAT GTT GTG GGT CAG ^{5m}CGC ATG ATA GTG TA-3′, ATDBio Ltd), ^{5m}C double-stranded DNA (5′-ACC AC^{5m}C GGT GGT-3′, ATDBio Ltd), anti-5-hydroxymethylcytosine (^{5hm}C) rabbit antibody (pAb, Active Motif, Cat# 39769, RRID: AB_10013602), 8-hydroxy-5-quinoline carboxylic acid (IOX1, Cayman Chemicals, Cat# 11572), *N*–oxalylglycine (NOG, Cayman chemicals, Cat# 13944), Agilent RapidFire cartridge C18 (type C, Cat# G9205A). Linear FLAG, TAT, and R8 peptides were purchased from GL Biochem (Shanghai).

4.1.1. General experimental conditions

Water was purified using Milli-Q® Reference Water Purification System with Quantum® TEX Polishing Cartridge and a Millipak® Express 40 Filter. Biochemical assays were conducted at room temperature unless stated otherwise. All biochemical activity data were analysed using GraphPad Prism.

4.2. Chemistry

4.2.1. General method for the synthesis of peptides

Peptides were produced (50–100 μmol) using standard solid-phase peptide synthesis applying Fmoc-type chemistry on a Liberty Blue (CEM) peptide synthesiser using the manufacturer's recommended methods. Synthesis was performed in DMF on Rink amide resin using DIC and OxymaPure as activators. Peptides designated for cyclisation were capped with an *N*–terminal chloroacetyl group using chloroacetic anhydride (10 equiv.) in DMF (5 mL) for 2 h (RT), followed by a further addition of chloroacetic anhydride (5 equiv.) and a final 1 h incubation. Linear peptide TiP1.L was capped with acetic anhydride following the same protocol. The resin was washed using CH_2Cl_2 (3 × 15 mL) following oligomerisation; peptides were cleaved from the resin and acid-labile groups were removed using 5 mL of a mixture of 1,3-dimethoxybenzene/triisopropylsilane/water/TFA (2.5:2.5:2.5:92.5) for 3 h. The suspension was filtered, and the cleaved peptide was triturated from Et_2O (–20 °C, 16 h). The precipitate was pelleted by centrifugation (3,082 × g, 10 min, 4 °C) and supernatant was removed. The trituration process was repeated for a total of three rounds. The remaining crude peptide was resuspended in a minimal amount of a water/acetonitrile mixture and volatiles were removed by lyophilisation.

4.2.2. Peptide cyclisation

Lyophilised crude peptides were suspended in DMSO (30 mg/mL) and dissolution was achieved by sonication (10 min, 35 °C). The pH of the mixture was adjusted to pH 9 using *N*,*N*–diisopropylethylamine (DIPEA). The solution was incubated for 1.5 h (40 °C) and cyclisation was monitored by MALDI-TOF MS. The reaction was quenched by the addition of TFA to give a pH of 4–5.

4.2.3. Semi-preparative HPLC

A DMSO solution of each crude cyclised peptide was filtered (0.45 μm filter) and purified using a Phenomenex Gemini® 5 μm NX-C18 110 Å column and a Shimadzu Prominence semi-preparative HPLC machine using a water/acetonitrile solvent system supplemented with TFA (0.1% v/v). Selected fractions based on MALDI-TOF MS analysis were pooled and lyophilised to yield the purified product. Peptide purity was determined based on UV absorbance (220 nm) using an LC-MS Water ACQUITY UPLC in conjunction with MS analysis using a Xevo G2-XS Q-TOF machine in positive electrospray ionisation mode. The concentrations of peptides with poor water solubility were measured using a NanoDrop One Microvolume UV–Vis spectrophotometer (normalised using the molar extinction coefficient at 280 nm wavelength). Water-soluble peptide concentrations were determined by ^{1}H NMR using a Bruker Avance III 700 MHz machine with an internal standard TSP-[^{2}H]$_4$.

4.2.4. MALDI-TOF MS analysis

A saturated matrix solution was prepared by sonication (10 min) of α-cyano-4-hydroxycinnamic acid (αCCN, 10 mg/mL) in water/acetonitrile (1:1, 0.1% v/v TFA). The matrix mixture (1.0 μL) was deposited on a MALDI-TOF target plate and sample (1.0 μL) was added. The spots were air-dried at room temperature and samples were analysed by Bruker MALDI-TOF Autoflex maX mass spectrometer recording 700–3,500 Da range in positive reflectron mode.

4.3. Biochemical assays

4.3.1. Acoustic dispensing of inhibitors

Inhibitor dilution series were prepared as DMSO stocks and plated onto ProxiPlates™ for AlphaScreen assays or Greiner 384-well polypropylene (PP) plates for SPE-MS assays using an Echo 550 acoustic liquid handler (Labcyte). DMSO stocks were dispensed in increments of 2.5 nL up to a final volume of 100 nL for AlphaScreen and 250 nL for SPE-MS (1% DMSO in final assay volume). Where required, a DMSO backfill was performed up to 100 nL or 250 nL, respectively.

4.3.2. AlphaScreen assays for TETs

Inhibition of TET activity was measured by AlphaScreen-based assays (PerkinElmer) according to literature procedures.[32,34] In brief, compound dilution series were prepared by acoustic Echo dispensing on a ProxiPlate™ from a DMSO source stock, as described in Section 4.3.1. A mixture of AlphaScreen beads (1:62.5 dilution) and anti-^{5hm}C antibody (1:2,000 dilution) was prepared in AlphaScreen buffer containing HEPES (50 mM, pH 7.3), NaCl (150 mM), BSA (0.1% w/v), and Tween®20 (0.01% v/v), and incubated for at least 30 min. To the inhibitor plate was added 5 μL of 2 nM TET1$_{CD}$, 2 nM TET2$_{CD\Delta LCI}$, 10 nM TET3$_{CD}$, or 2 nM mTet1$_{CD}$ in AlphaScreen buffer; the mixtures were then

incubated for 10 min. 5 μL of co-factor/co-substrate solution containing sodium L-ascorbate (200 μM), $(NH_4)_2Fe(SO_4)_2$ (20 μM), 2OG (20 μM), and ^{5m}C single-stranded DNA (10 nM) in AlphaScreen buffer was then added. The enzymatic reaction was allowed to run for 30 min ($TET1_{CD}$), 10 min ($TET2_{CD\Delta LCI}$), 10 min ($TET3_{CD}$), or 9 min ($mTet1_{CD}$), and quenched by EDTA addition (30 mM EDTA, 358 mM NaCl, pH 4.2). 5 μL of AlphaScreen bead/anti-^{5hm}C antibody mixture was added, the plate was incubated for 45–60 min, and luminescence was measured using a PHERAstar FS (BMG Labtech, AlphaScreen 680 570 module). AlphaScreen interference assays were conducted in the absence of TET enzyme; DNA substrate consisted of a combination of ^{5m}C single-stranded DNA (8.5 nM) and ^{5hm}C single-stranded DNA (1.5 nM) to simulate enzymatic turnover. All steps involving AlphaScreen beads were carried out under subdued lighting.

4.3.3. AlphaScreen assay for KDM5B and KDM6B

Cross-screening of TiP1 against KDM5B and KDM6B was conducted according to a literature procedure.[51]

4.3.4. SPE-MS assay for $TET2_{CD\Delta LCI}$

Inhibition of $TET2_{CD\Delta LCI}$ activity was measured by SPE-MS according to a literature procedure.[32] In brief, compound dilution series were prepared by acoustic Echo dispensing on a Greiner 384-well polypropylene (PP) plate from a DMSO source stock, as described in Section 4.3.1. 12.5 μL of $TET2_{CD\Delta LCI}$ (600 nM) in SPE-MS buffer containing HEPES (50 mM, pH 7.3) was added to the plate, which was then incubated for 10 min. Enzymatic reaction was initiated by the addition of 12.5 μL DNA and cofactor solution in SPE-MS buffer containing ^{5m}C double-stranded DNA (2.0 μM), sodium L-ascorbate (400 μM), $(NH_4)_2Fe(SO_4)_2$ (50 μM), and 2OG (50 μM). The enzymatic reaction was allowed to run for 12 min and quenched by NOG addition (25 μL, 2 mM in water). Samples were analysed by Agilent RapidFire 365 coupled to an Agilent 6550 iFunnel Q-TOF mass spectrometer using a C18 cartridge with solvent A (6 mM octylammonium acetate in water) and solvent B (80% v/v acetonitrile in water). Enzymatic activity was determined by measuring the levels of ^{5hm}C double-stranded DNA (+16 Da) relative to ^{5m}C double-stranded DNA.

4.3.5. SPE-MS assays for FIH, PHD2, and ASPH

Cross-screening of TiP1 against FIH,[35,52] PHD2,[35] and ASPH[36] was conducted according to literature procedures. Substrate peptides were prepared as *C*–terminal amides by GL Biochem (Shanghai) Ltd with HIF-1α *C*–terminal transactivation domain fragment (HIF-1α C-$TAD_{788\text{-}822}$) for FIH; HIF-1α *C*–terminal oxygen-dependent degradation domain fragment (HIF-1α $CODD_{556\text{-}574}$) for PHD2; human Factor X cyclic peptide fragment (hFX-$CP_{101\text{-}119}$) for ASPH. Peptide hydroxylation (+16 Da mass shift) was monitored by SPE-MS.

4.4. Protein production

Recombinant $TET2_{CD\Delta LCI}$ (D1129–G1936 with 1481–1844 replaced by a 3 × GGGGS linker),[42] PHD2 (P181–F426),[53] KDM6B (D1141–E1590),[54] FIH (M1–N349),[52,55] and ASPH (R315–I758)[56] were produced using *E. coli* expression systems following reported procedures. Recombinant KDM5B (M1–822)[51] and $TET1_{CD}$ (E1418–V2136)[32] were produced using Sf9 baculovirus expression systems, while recombinant $TET3_{CD}$ (E824–I1795)[32] was produced using mammalian cells following reported procedures. Recombinant murine $Tet1_{CD}$ (E1367-V2039) was produced using the High Five baculovirus expression system following reported procedures.[57]

4.5. TET inhibition immunofluorescence assay

The cellular TET inhibition assay was conducted according to a literature procedure,[32] using doxycycline-inducible stable U2OS cells expressing the gene coding for the catalytic domain of wild-type TET1 (E1418–V2136). In brief, 5,000 cells per well were seeded into clear-bottom 96-well plates (CellCarrier Ultra-96, Perkin-Elmer) in DMEM media supplemented with Tet system-approved FBS (10%), penicillin G (50 IU/mL), streptomycin (50 μg/mL), and L-glutamine (2 mM), and incubated for 4 h at 37 °C. Cells were induced with doxycycline (1 μg/mL) and dosed with compounds (1% DMSO final) for 24 h. Cells were then fixed, permeabilised, blocked (FBS (3%) in PBS), and incubated with primary anti-^{5hm}C rabbit polyclonal antibody (1:500 dilution) and anti-FLAG mouse monoclonal antibody (Sigma, Cat#: F1804, 1:1000 dilution) for 16 h. Secondary antibody in FBS (3%) in PBS (anti-rabbit Alexa® 647 conjugate and anti-mouse Alexa® 568 conjugate, Life Technologies, 1:500 dilution) was incubated for 1 h. Cell nuclei were stained with 4′,6-diamidino-2-phenylindole (DAPI, Invitrogen). Cell imaging was performed using Cell Discoverer 7 high-throughput (Zeiss) system. ^{5hm}C staining intensities (Alexa Fluor® 647) of FLAG-TET1 expressing cells post-compound treatment were determined based on mean fluorescence (SEM and N).

CRediT authorship contribution statement

Klemensas Šimelis: Writing – review & editing, Writing – original draft, Visualization, Methodology, Investigation, Data curation. **Hilal Saraç:** Methodology, Investigation, Data curation. **Eidarus Salah:** Resources, Methodology. **Kosuke Nishio:** Data curation. **Tom E. McAllister:** Writing – review & editing, Visualization, Formal analysis. **Thomas P. Corner:** Writing – review & editing, Data curation. **Anthony Tumber:** Data curation. **Roman Belle:** Writing – review & editing, Writing – original draft, Supervision, Methodology. **Christopher J. Schofield:** Writing – review & editing, Supervision. **Hiroaki Suga:** Writing – review & editing, Supervision. **Akane Kawamura:** Writing – review & editing, Visualization, Supervision, Project administration, Funding acquisition, Formal analysis, Conceptualization.

Declaration of competing interest

The authors declare that they have no known competing financial interests or personal relationships that influenced the work reported in this paper.

Data availability

Data will be made available on request.

Acknowledgements

We thank Prof. Chunxiao Song (U. Oxford) for providing mTet1 protein, Dr Lennart Brewitz (Schofield group, U. Oxford) for providing ASPH protein, and Giorgia Fiorini (Schofield group, U. Oxford) for providing PHD2 protein. We are grateful to Prof. Tom Brown (U. Oxford) and ATDBio for the provision of DNA substrates used in this study, and Prof. Yanhui Xu (State Key Laboratory of Genetic Engineering, Fudan University, China) for the plasmid coding for His_6-FLAG-SUMO-tagged $TET2_{CD\Delta LCI}$.

Funding sources

This work was supported by European Research Council (ERC) under the European Union's Horizon 2020 research and innovation programme [679479, 101003111 to AK] and Cancer Research UK [C8717/A28285, C5255/A18085]. KS is grateful to the EPSRC Centre for Doctoral Training in Synthesis for Biology and Medicine (EP/L015838/1) for a studentship, generously supported by AstraZeneca, Diamond Light Source, Defence Science and Technology Laboratory, Evotec, GlaxoSmithKline, Janssen, Novartis, Pfizer, Syngenta, Takeda, UCB, and Vertex. For the purpose of Open Access, the author has applied a CC BY public copyright licence to any Author Accepted Manuscript (AAM)

version arising from this submission.

Contributions

KŠ synthesised the peptides, produced $TET2_{CD\Delta LCI}$ protein, and carried out biochemical assays for TET1–3 and mTet1. HS carried out cellular TET inhibition assays. ES produced TET1, TET3, KDM5B, 6B, and FIH proteins. NK carried out the RaPID selection, identified initial hits, and carried out the NGS under the supervision of HS. TEM analysed NGS data from TET1 RaPID selection. TPC tested TiP1 against PHD2, FIH, and ASPH, and AT tested TiP1 against KDM5B and 6B. CJS supervised TPC and AT. RB purified ^{5m}C and ^{5hm}C DNA substrates for TET AS assay. KS, RB, and AK analysed the data and wrote the manuscript with input from all authors. AK supervised and administrated the project.

Appendix A. Supplementary data

Supplementary data to this article can be found online at https://doi.org/10.1016/j.bmc.2024.117597.

References

1. Rivera RM, Bennett LB. Epigenetics in humans: An overview. *Curr Opin Endocrinol Diabetes Obes*. 2010;17:493–499.
2. Tahiliani M, et al. Conversion of 5-methylcytosine to 5-hydroxymethylcytosine in mammalian DNA by MLL partner TET1. *Science*. 2009;324:930–935.
3. Ito S, et al. Tet proteins can convert 5-methylcytosine to 5-formylcytosine and 5-carboxylcytosine. *Science*. 2011;333:1300–1303.
4. Breiling A, Lyko F. Epigenetic regulatory functions of DNA modifications: 5-methylcytosine and beyond. *Epigenetics Chromatin*. 2015;8:24.
5. Li F, et al. 5-formylcytosine yields DNA-protein cross-links in nucleosome core particles. *J Am Chem Soc*. 2017;139:10617–10620.
6. Raiber EA, et al. 5-formylcytosine organizes nucleosomes and forms schiff base interactions with histones in mouse embryonic stem cells. *Nat Chem*. 2018;10:1258–1266.
7. Song CX, et al. Genome-wide profiling of 5-formylcytosine reveals its roles in epigenetic priming. *Cell*. 2013;153:678–691.
8. Kellinger MW, et al. 5-formylcytosine and 5-carboxylcytosine reduce the rate and substrate specificity of RNA polymerase II transcription. *Nat Struct Mol Biol*. 2012;19:831–833.
9. Wang L, et al. Molecular basis for 5-carboxycytosine recognition by RNA polymerase II elongation complex. *Nature*. 2015;523:621–625.
10. Lu X, et al. Base-resolution maps of 5-formylcytosine and 5-carboxylcytosine reveal genome-wide DNA demethylation dynamics. *Cell Res*. 2015;25:386–389.
11. Liu D, Li G, Zuo Y. Function determinants of TET proteins: The arrangements of sequence motifs with specific codes. *Brief Bioinform*. 2019;20:1826–1835.
12. Zhang W, et al. Isoform switch of TET1 regulates DNA demethylation and mouse development. *Mol Cell*. 2016;64:1062–1073.
13. Adam S, et al. Flanking sequences influence the activity of TET1 and TET2 methylcytosine dioxygenases and affect genomic 5hmC patterns. *Commun. Biol.* 2022;5:92.
14. Lian H, Li WB, Jin WL. The emerging insights into catalytic or non-catalytic roles of TET proteins in tumors and neural development. *Oncotarget*. 2016;7:64512–64525.
15. Zhang Q, et al. Tet2 is required to resolve inflammation by recruiting Hdac2 to specifically repress IL-6. *Nature*. 2015;525:389–393.
16. Williams K, et al. TET1 and hydroxymethylcytosine in transcription and DNA methylation fidelity. *Nature*. 2011;473:343–349.
17. Gu TP, et al. The role of Tet3 DNA dioxygenase in epigenetic reprogramming by oocytes. *Nature*. 2011;477:606–612.
18. Yamaguchi S, Shen L, Liu Y, Sendler D, Zhang Y. Role of Tet1 in erasure of genomic imprinting. *Nature*. 2013;504:460–464.
19. Huang Y, et al. Distinct roles of the methylcytosine oxidases Tet1 and Tet2 in mouse embryonic stem cells. *Proceedings of the National Academy of Sciences of the United States of America*. 2014;111:1361–1366.
20. Lan J, et al. Functional role of tet-mediated RNA hydroxymethylcytosine in mouse ES cells and during differentiation. *Nat Commun*. 2020;11:4956.
21. Yang H, et al. Tumor development is associated with decrease of TET gene expression and 5-methylcytosine hydroxylation. *Oncogene*. 2013;32:663–669.
22. Feng Y, Li X, Cassady K, Zou Z, Zhang X. TET2 function in hematopoietic malignancies, immune regulation, and DNA repair. *Front Oncol*. 2019;9:210.
23. Ono R, et al. LCX, leukemia-associated protein with a CXXC domain, is fused to MLL in acute myeloid leukemia with trilineage dysplasia having t(10;11)(q22;q23). *Cancer Res*. 2002;62:4075–4080.
24. Maiti A, Drohat AC. Thymine DNA glycosylase can rapidly excise 5-formylcytosine and 5-carboxylcytosine: Potential implications for active demethylation of CpG sites. *J Biol Chem*. 2011;286:35334–35338.
25. Iwan K, et al. 5-formylcytosine to cytosine conversion by C-C bond cleavage in vivo. *Nat Chem Biol*. 2018;14:72–78.
26. Kamińska E, Korytiaková E, Reichl A, Müller M, Carell T. Intragenomic decarboxylation of 5-Carboxy-2′-deoxycytidine. *Angew. Chemie - Int. Ed.* 2021;60:23207–23211.
27. Liutkevičiutė Z, et al. Direct decarboxylation of 5-carboxylcytosine by DNA C5-methyltransferases. *J Am Chem Soc*. 2014;136:5884–5887.
28. Baader E, Tschank G, Baringhaus KH, Burghard H, Gunzler V. Inhibition of prolyl 4-hydroxylase by oxalyl amino acid derivatives in vitro, in isolated microsomes and in embryonic chicken tissues. *Biochem J*. 1994;300:525–530.
29. Sudhamalla B, Dey D, Breski M, Islam K. A rapid mass spectrometric method for the measurement of catalytic activity of ten-eleven translocation enzymes. *Anal Biochem*. 2017;534:28–35.
30. Hopkinson RJ, et al. 5-Carboxy-8-hydroxyquinoline is a broad spectrum 2-oxoglutarate oxygenase inhibitor which causes iron translocation. *Chem Sci*. 2013;4:3110–3117.
31. King ONF, et al. Quantitative high-throughput screening identifies 8-hydroxyquinolines as cell-active histone demethylase inhibitors. *PLoS One*. 2010;5:e15535.
32. Belle R, et al. Focused screening identifies different sensitivities of human TET oxygenases to the oncometabolite 2-hydroxyglutarate. *J Med Chem*. 2024. https://doi.org/10.1021/acs.jmedchem.3c01820.
33. Guan Y, et al. A therapeutic strategy for preferential targeting of TET2-mutant and TET dioxygenase-deficient cells in myeloid neoplasms. *Cancer Discov*. 2021;2:146–161.
34. Nishio K, et al. Thioether macrocyclic peptides selected against TET1 compact catalytic domain inhibit TET1 catalytic activity. *Chembiochem*. 2018;19:979–985.
35. Holt-Martyn JP, et al. Structure-activity relationship and crystallographic studies on 4-hydroxypyrimidine HIF prolyl hydroxylase domain inhibitors. *ChemMedChem*. 2020;15:270–273.
36. Brewitz L, Tumber A, Pfeffer I, McDonough MA, Schofield CJ. Aspartate/asparagine-β-hydroxylase: a high-throughput mass spectrometric assay for discovery of small molecule inhibitors. *Sci Rep*. 2020;10:8650.
37. Hu X, et al. Epigenetic drug screen identified IOX1 as an inhibitor of Th17-mediated inflammation through targeting TET2. *EBioMedicine*. 2022;86, 104333.
38. Matsson P, Kihlberg J. How big is too big for cell permeability? *J Med Chem*. 2017;60:1662–1664.
39. Appiah Kubi G, Dougherty PG. & Pei D. Designing Cell-Permeable Macrocyclic Peptides. In: Goetz G. editor. Cyclic Peptide Design. New York, Springer; 2019. Pp. 41–59. https://doi.org/10.1007/978-1-4939-9504-2_3.
40. Jones AT, Sayers EJ. Cell entry of cell penetrating peptides: Tales of tails wagging dogs. *J Control Release*. 2012;161:582–591.
41. Kawamura A, et al. Highly selective inhibition of histone demethylases by de novo macrocyclic peptides. *Nat Commun*. 2017;8:14773.
42. Hu L, et al. Crystal structure of TET2-DNA complex: Insight into TET-mediated 5mC oxidation. *Cell*. 2013;155:1545–1555.
43. Pillaiyar T, Manickam M, Namasivayam V, Hayashi Y, Jung SH. An overview of severe acute respiratory syndrome-coronavirus (SARS-CoV) 3CL protease inhibitors: Peptidomimetics and small molecule chemotherapy. *J Med Chem*. 2016;59:6595–6628.
44. Buckley DL, et al. Targeting the von hippel-Lindau E3 ubiquitin ligase using small molecules to disrupt the VHL/HIF-1α interaction. *J Am Chem Soc*. 2012;134:4465–4468.
45. McAllister TE, et al. Non-competitive cyclic peptides for targeting enzyme-substrate complexes. *Chem Sci*. 2018;9:4569–4578.
46. Coleman OD, et al. Cyclic peptides target the aromatic cage of a PHD-finger reader domain to modulate epigenetic protein function. *Chem Sci*. 2023;14:7136–7146.
47. Rivas MP, et al. TET upregulation leads to 5-hydroxymethylation enrichment in hepatoblastoma. *Front Genet*. 2019;10:553.
48. Shirai K, et al. TET1 upregulation drives cancer cell growth through aberrant enhancer hydroxymethylation of HMGA2 in hepatocellular carcinoma. *Cancer Sci*. 2021;112:2855–2869.
49. Collignon E, et al. Immunity drives TET1 regulation in cancer through NF-kB. *Sci Adv*. 2018;4:eaap7309.
50. Good CR, Panjarian S, Kelly AD, Madzo J. TET1-mediated hypomethylation activates oncogenic signaling in triple-negative breast cancer. *Cancer Res*. 2018;78:4126–4137.
51. Johansson C, et al. Structural analysis of human KDM5B guides histone demethylase inhibitor development. *Nat Chem Biol*. 2016;12:539–545.
52. Nakashima Y, Brewitz L, Tumber A, Salah E, Schofield CJ. 2-oxoglutarate derivatives can selectively enhance or inhibit the activity of human oxygenases. *Nat Commun*. 2021;12:6478.
53. Chowdhury R, et al. Structural basis for binding of hypoxia-inducible factor to the oxygen-sensing prolyl hydroxylases. *Structure*. 2009;17:981–989.
54. Rose NR, et al. Plant growth regulator daminozide is a selective inhibitor of human KDM2/7 histone demethylases. *J Med Chem*. 2012;55:6639–6643.
55. Hewitson KS, et al. Hypoxia-inducible factor (HIF) asparagine hydroxylase is identical to factor inhibiting HIF (FIH) and is related to the cupin structural family. *J Biol Chem*. 2002;277:26351–26355.
56. Pfeffer I, et al. Aspartate/asparagine-β-hydroxylase crystal structures reveal an unexpected epidermal growth factor-like domain substrate disulfide pattern. *Nat Commun*. 2019;10:4910.
57. Yu M, et al. Tet-assisted bisulfite sequencing of 5-hydroxymethylcytosine. *Nat Protoc*. 2012;7:2159–2170.